JOURNAL OF PROPULSION AND POWER
Vol. 25, No. 4, July–August 2009

Reaction Mechanism of Aluminum-Particle–Air Detonation

Fan Zhang* and Keith Gerrard†
Defence R&D Canada – Suffield, Medicine Hat, Alberta T1A 8K6, Canada
and
Robert C. Ripley‡
Martec Limited, Halifax, Nova Scotia B3J 3J8, Canada

DOI: 10.2514/1.41707

Both in-tube and unconfined experimental evidence showed strong dependence of micrometric aluminum–air detonability on initial pressure and highly nonlinear behavior of abrupt deflagration-to-detonation transition, thus indicating dependence of the aluminum reaction mechanism of the detonation waves on chemical kinetics. On the other hand, the observed aluminum–air detonation manifested itself in a weak transverse wave structure, as revealed by the small-amplitude oscillation that rapidly degenerates behind the shock front in the pressure histories. This suggests a functional dependence that is weaker than the nonlinear Arrhenius kinetic behavior for the later aluminum combustion. Hence, a surface kinetic oxidation and diffusion hybrid reaction model with a degree of condensed detonation products was suggested, and the unsteady two-phase fluid dynamics modeling showed the success of the hybrid reaction model, capable of capturing both the kinetics-limited transient processes of detonation initiation, abrupt deflagration-to-detonation transition and detonation instability, and the diffusion-limited combustion of aluminum in the long reaction zone, supporting the weak transverse wave structure.

Nomenclature

a_e	=	equilibrium sound speed, m/s
a_g	=	phase-frozen sound speed, m/s
C	=	mole concentration, mol/m^3
C_D	=	drag coefficient
D	=	detonation velocity, m/s
D_g	=	gas-phase diffusivity, m^2/s
d_p	=	particle diameter, m
E	=	activation energy, J/mol
e	=	specific internal energy, J/kg
f_p	=	rate of momentum transfer between the solid and the gas phase, N/m^3
J_p	=	rate of mass transfer between the particles and the gas phase, kg/m^3 · s
K	=	diffusion reaction coefficient, s/m^2
k	=	mass depletion flux, kg/m^2 · s
k_d	=	rate coefficient of diffusion reaction, kg · m/mol · s
k_s	=	rate coefficient of kinetic reaction, kg · m/mol · s
k_0	=	kinetic reaction coefficient, kg · m/mol · s
L_b	=	latent heats of evaporation, J/mol
L_m	=	latent heats of melting, J/mol
Nu	=	Nusselt number
n_p	=	particle number density, 1/m^3
Pr	=	gas-phase Prandtl number
p	=	pressure, N/m^2
Q_p	=	rate of heat transfer between the particles and the gas phase, J/m^3 · s
q_p	=	heat release of particles, J/kg
R	=	universal gas constant, J/mol · K
Re	=	two-phase Reynolds number
r_p	=	particle radius, m
T	=	temperature, K
T_{ign}	=	particle ignition temperature, K
t_b	=	particle burning time, s
u	=	flow velocity, m/s
W	=	molecular weight, g/mol
w	=	species reaction rate, kg/m^3 · s
x	=	distance in the shock-propagation direction, m
Y	=	mass fraction of species
λ_g	=	thermal conductivity of the gas phase, W/m · K
ν	=	stoichiometric coefficient
ρ	=	material density, kg/m^3
σ	=	partial density or mass concentration, kg/m^3
ϕ	=	volume fraction
Ψ_p	=	rate of particle number production, 1/m^3 · s

Subscripts

g	=	gas-phase index
oxi	=	index for oxidizing gases
p	=	particle-phase index
s	=	index for particle surface
0	=	initial state

Received 19 October 2008; revision received 24 February 2009; accepted for publication 25 February 2009.

*Senior Scientist, P.O. Box 4000, Station Mainfan.zhang@drdc-rddc.gc.ca; Adjunct Professor, University of Waterloo, Department of Mechanical Engineering, Waterloo, ON N2L 3G1, Canada.

†Senior Technologist, 400-1888 Brunswick Street, P.O. Box 4000, Station Main.

‡Senior Research Engineer, 400-1888 Brunswick Street.

I. Introduction

THE detonability of fine aluminum (Al) particles suspended in air is an important fundamental problem in understanding the explosion limit in a metal-particle–gas flow. Experiments showed that Al–air detonation at atmospheric conditions is only feasible for a particle characteristic size of less than a few micrometers (and in large tubes, 0.12–0.3 m in diameter), thus indicating a relative insensitivity to detonation [1–3].

Al particles possess a high-melting-point oxide coating that must be melted or cracked open before aluminum can react. Lacking sound knowledge of the Al reaction mechanism under detonation conditions, the droplet diffusion combustion theory has been often applied to Al-particle–gas detonation problems [2,4]. The diffusion theory states that the particle burning time is proportional to a power of its initial diameter, $t_b \sim d_{p0}^n$ $(n = 2)$, as the temperature of a

particle exceeds the oxide melting point [5]. The theory assumes infinite kinetics and is essentially independent of temperature and pressure. It applies according to the classic experimental observations for combustion of large Al particles in quiescent atmospheres [6]. Under conditions of 10^1–10^2 atm and 1–50 μm particles, however, it has been found that the burning rate of aluminum particles is greater than that in 1 atm air, thus resulting in a dependence on pressure but a smaller power n between 1 and 2 [7–11]. For the combustion of Al particles smaller than 30 μm, even under atmospheric conditions, the diffusion theory could lead to an overprediction of the burning rate [12–14]. The power $n < 2$ implies the contribution of finite chemical kinetics and possibly convective flow effects [5]. Because the burning-aluminum mass flux in the particle radial direction is inversely proportional to particle radius (yielding $t_b \sim d_{p0}^2$) in the diffusional transport and independent of particle radius (yielding $t_b \sim d_{p0}$) in the kinetic process, the diffusional transport rates approach infinity as particle diameter approaches zero, whereas kinetic process rates do not increase with decreasing particle size. Therefore, at sufficiently small particle diameters, the use of the d^2 law becomes incorrect and the particle combustion must become kinetics-dependent.

Interaction with a shock wave and subsequent flow could furthermore change the physical properties of the Al particles and consequently influence the ignition and reaction of particles [15–20]. Whereas in quiescent or low-speed flow, a threshold ignition temperature was observed to be above 2100 K for 2–30 μm atomized aluminum particles at 6–11 bar [20], Borisov et al. [15] reported a drop of the ignition temperature to about 1400 K for 15–20 μm Al particles, and Boiko et al. [16] showed ignition at 1260 K under appropriate Al concentration after a reflected shock. The shock ignition temperature would be expected to be even lower for 1–2 μm particles. A temperature of 1000–1400 K results in a vapor pressure of 10^{-5}–10^{-1} Pa only, thus further indicating the questionability of diffusion-limited evaporation reaction in shocked conditions.

Because aluminum–air detonation only occurs for a particle characteristic size less than a few micrometers and the particles burn under the shocked and the subsequent detonation conditions, one would expect that the limited kinetics affects the aluminum reaction. Application of the temperature-independent and weakly pressure-dependent diffusion-controlled Al reaction theory seems to prevent an appropriate description for the mechanism of the aluminum–air detonation initiation and the deflagration-to-detonation transition (DDT). In this paper, the importance of exploring kinetic-dependent approaches will be addressed from recent experimental evidence of the aluminum–air detonation. This includes a strong dependence of Al–air detonation on initial pressure in tubes and highly nonlinear abrupt DDT, both in tubes and in unconfined Al–air clouds without the influence of tube confinement. On the other hand, the observed aluminum–air detonation exhibits a weak transverse wave structure, as revealed by the small oscillation amplitude in the pressure histories. Considering these experimental observations, a hybrid model of surface kinetics-diffusion reaction is introduced in an attempt to understand the Al reaction mechanism in the process of detonation initiation and DDT as well as in the detonation structure.

II. Pressure Dependence of Al–Air Detonation

A horizontal detonation tube of 80 mm internal diameter was used to study the pressure dependence of Al–air detonation [21]. The tube consisted of a 9.6 m test section connected to a 3 m relieve section by an aluminum diaphragm. The test section was equipped with a dispersion system that provided a fairly uniform Al-particle suspension at an elevated initial pressure. An RP-83 detonator made by Reynolds Industries Systems, Inc., was employed for initiation and installed at the beginning of the test section. The detonator contained 0.08 g pentaerythritol tetranitrate (PETN) and 1.031 g cyclotrimethylenetrinitramine (RDX) with binder and provided 6 kJ initiation energy. The polychlorinated biphenyl (PCB) pressure transducers were installed along the tube.

The test Al particles chosen were a nanometric grade of Al known as Alex, supplied by Argonide Corporation and a micrometric grade of atomized Al known as H-2 with a mean diameter of 1.6 μm by number and a mean diameter of 3.3 μm by weight, supplied by Valimet, Inc. The shape and particle-size distribution are illustrated in scanning electron micrographs (SEMs), as shown in Fig. 1. Alex is manufactured by an exploding-wire process and has a mean particle diameter of approximately 100 nm. Noting that the Alex particles are passivated with an oxide coating to a mass fraction of about 10%, the detonation performance with Alex is expected to be less energetic than that of pure aluminum.

The effect of initial pressure on DDT in the 100 nm Al–air mixtures is displayed in Figs. 2 and 3 by pressure records along the tube length at an initial Al-particle concentration of 400 $\mathrm{g/m^3 \cdot atm}$. Note that a nominal particle concentration is introduced here with a unit of grams per cubic meter and per atm to keep the same equivalence ratio in air for various initial pressures. Owing to the initiation source, a blast wave is developed in the early stage with a shock velocity of 860–930 m/s. At an initial pressure $p_0 = 1$ atm, multiple compression waves supported by energy release from the Al–air flame appear behind the shock front during the DDT process (Fig. 2). At a distance larger than 8 m, a local explosion takes place and is amplified behind the shock front, leading to abrupt transition to detonation at the end of the test section with an overdriven peak pressure of $p/p_0 = 45.0$. Thereafter, a reflected wave off the diaphragm at the end propagates back into the test section. Note that all the abrupt DDT processes shown in this paper complete within a scaled distance of only a few characteristic cell size of Al–air detonation.

When the initial pressure is increased to 1.5 atm, the abrupt transition to detonation takes place earlier (Fig. 3). At 8.3 m, the established overdriven detonation starts to relax toward a propagation velocity of 1650 m/s and a peak pressure of $p/p_0 = 35.0$ at the end of the test section. A further increase in initial pressure to 2–2.5 atm results in abrupt transition to an overdriven detonation at

Fig. 1 SEM of Al particles. Left: Alex with a mean diameter of 100 nm; middle: atomized H-2 with a mean diameter of 1.6 μm by number; right: Silberline DF-1667 Al flakes.

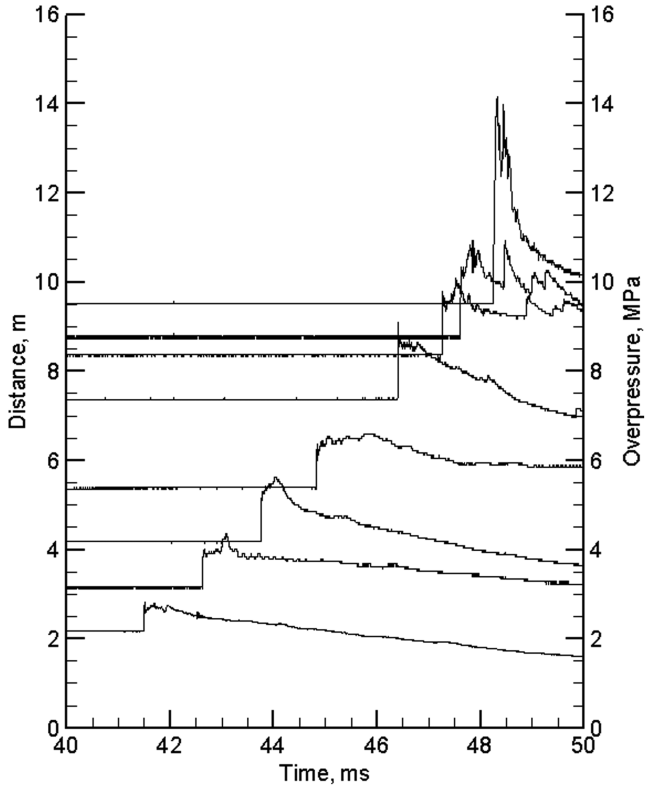

Fig. 2 DDT in a 400 g/m^3, 100 nm Al–air mixture at 1 atm.

6–7 m; it then relaxes toward an average propagation velocity of 1600 m/s and a corresponding peak pressure of $p/p_0 = 26.2$–31.6.

The detonation of the 100 nm Al–air mixtures manifests itself in the form of a spinning detonation in the tube. The single-head spinning structure is characterized by a primary oscillation period in the pressure history shown in Fig. 4 (at 8.72 m). As the initial

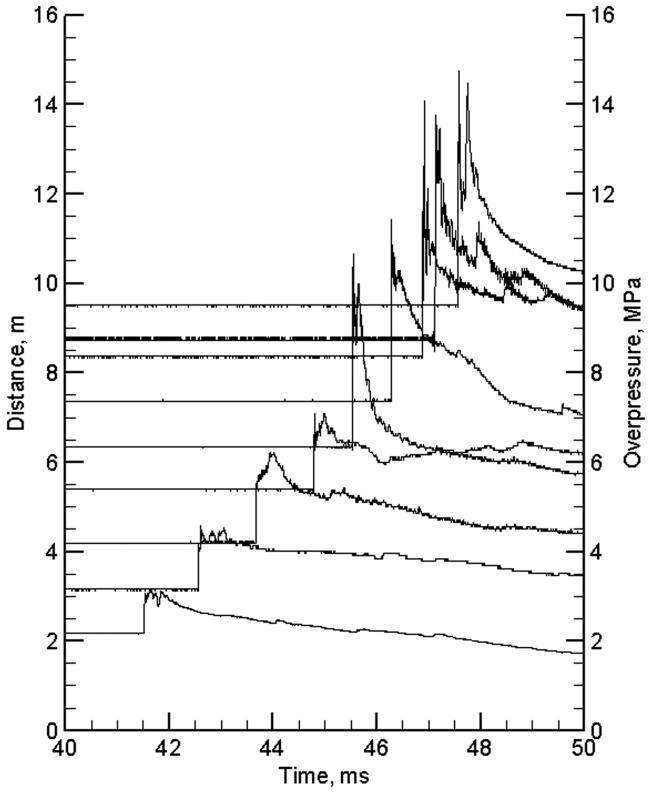

Fig. 3 DDT in a 400 g/m^3 · atm, 100 nm Al–air mixture at 1.5 atm.

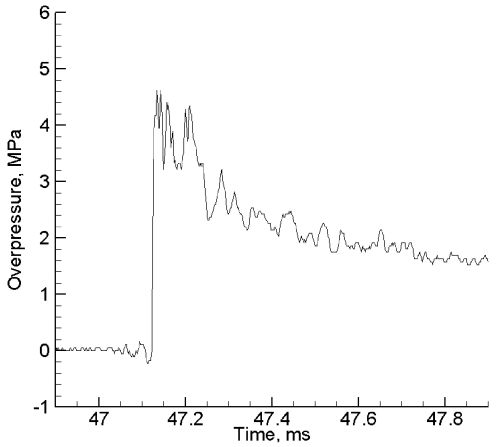

a) P_O = 1.5 atm

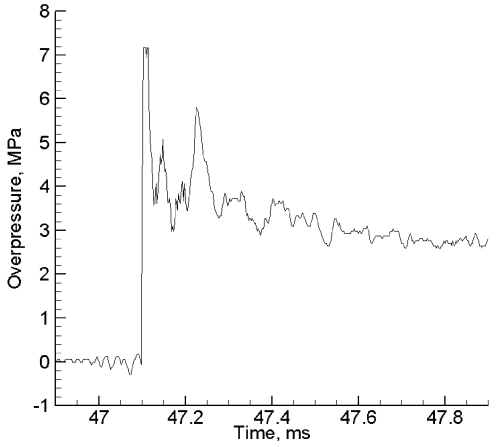

b) P_O = 2 atm

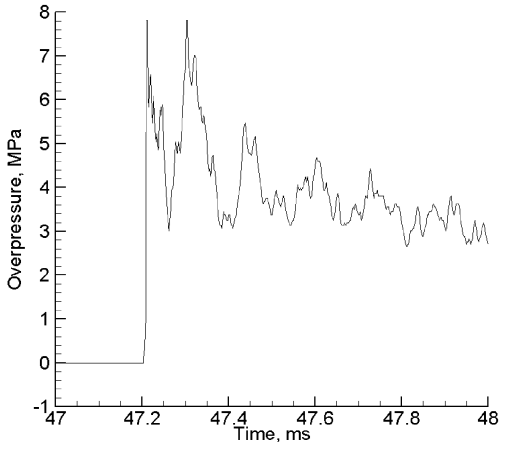

c) P_O = 2.5 atm

Fig. 4 Pressure oscillation at 8.72 m for 400 g/m^3 · atm, 100 nm Al–air mixture at 1.5–2.5 atm.

pressure increases, the primary oscillation becomes more distinguished, with an increase in amplitude, indicating a stronger transverse wave. A primary oscillation period of about 140 μs can be determined in the pressure history at $p_0 = 2.5$ atm. When multiplied by the propagation velocity at that location, this oscillation period results in a pitch of 0.23 m that is consistent with the smoke-foil record presented in [21].

As the mean diameter of Al particles was increased by an order of magnitude to 1.6 μm by number (H-2 atomized), at 2 atm and below, no transition to detonation occurred within the tube length. Instead, as indicated by the two tests at 2 atm in Fig. 5, the wave is accelerated to a propagation velocity far below the detonation velocity and then

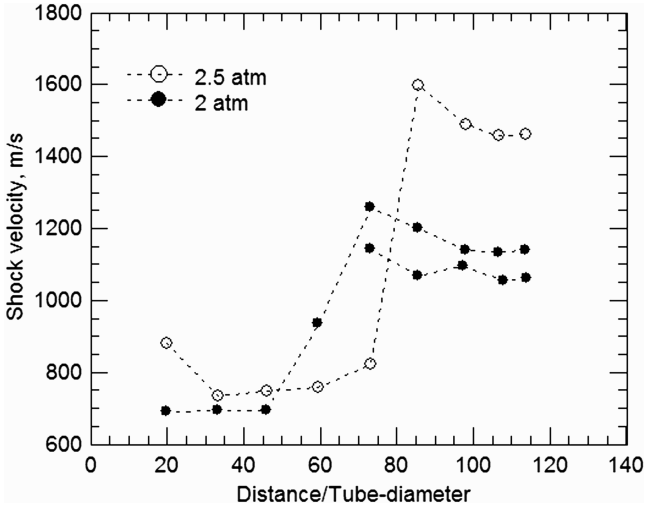

Fig. 5 Shock velocity versus distance for 500 g/m^3 · atm, H-2 Al–air at 2–2.5 atm.

propagates quasi-steadily at about 1100–1200 m/s toward the end of the tube. Such a shock-induced combustion wave has been referred to as *heterogeneous quasi-detonation* and its propagation mechanism has been discussed in [22]. Abrupt transition to a detonation was observed only when the initial pressure was increased to 2.5 atm, as indicated by the detailed pressure development along the tube in Fig. 6, for which the transition of the shock velocity is given in Fig. 5. After the transition, the overdriven detonation relaxes toward a stable mode with a peak pressure of $p/p_0 = 26.0$–28.4 and a propagation velocity of 1470 m/s. Although Fig. 5 displays the data for three experiments, an error range of the local detonation or quasi-steady shock velocities can be estimated to be about $\pm 5\%$ with respect to the local mean value of experiments.

In summary, both 100 nm and 1.6 μm Al–air DDT experiments show an abrupt transition to detonation via local explosions. An increase in initial pressure increases the detonation sensitivity of Al–air mixtures and reduces the detonation transition distance, whereas an increase in particle size decreases the detonation sensitivity. The oscillation structure of the 1.6 μm Al–air detonation is relatively weak, as shown in the pressure history in Fig. 7, similar to that for the 100 nm Al–air mixture at the 1.5 atm initial pressure (Fig. 4), thus indicating a weak transverse wave structure behind the shock front.

The theoretical equilibrium Chapman–Jouguet (C-J) detonation velocities and pressures are obtained using the Cheetah 2.0 code [23] over an initial pressure range between 1 and 5 atm, as displayed in Fig. 8. The detonation products in the equilibrium calculations include O_2, O, O_3, N_2, N, N_3, NO, NO_2, NO_3, N_2O, N_2O_3, N_2O_4, N_2O_5, Al, Al_2, AlN, AlO, AlO_2, Al_2O, Al_2O_2, Al (liquid), Al_2O_3 (liquid), Al (solid), AlN (solid), and Al_2O_3 (solid). The results show that an increase in initial pressure only causes a slight increase in equilibrium detonation velocity and pressure ratio p/p_0.

For the 100 nm Al–air detonation waves with spinning structures, the experimental detonation velocities at 1–2.5 atm are in agreement with the theoretical values within about 10%. The deviation from the equilibrium calculations conducted for the pure aluminum is expected, taking into account an oxide mass fraction of 10% for Alex powder. The equilibrium C-J pressures lie between the peaks and valleys of the experimental oscillatory pressure records, such as that shown in Fig. 4. The detonation velocities for the H-2 Al–air mixtures at 2.5 atm show a larger deficit with respect to the C-J equilibrium velocities (Fig. 8). This might be further caused by the heat loss to the tube wall, given the large reaction zone of the larger Al particles. In Fig. 8, error ranges of the experimental detonation velocities are estimated to be within $\pm 5\%$ with respect to the mean value at a given particle size and concentration.

III. Unconfined Al–Air Detonation

Very few experimental studies have been published for initiation of unconfined Al–gas detonation. Tulis [24] attempted to detonate 4.54 kg flaked Al explosively dispersed in air in a 1-m-high, 3-m-radius cylindrical cloud. The cloud was initiated near the center using 2.27 kg solid explosive; detonation was not observed and the ground pressure decayed from 1.8 to 0.9 MPa in radius from 1.3 to 2.7 m. Ingignoli et al. [25] detonated a rich flaked Al–oxygen cloud in a vertical cylindrical polyethylene bag, 1 m high and 0.7 m in diameter, initiated at the top using 150 g 2,4,6-trinitrotoluene, or TNT. The detonationlike wave observed near the bottom of the bag had a velocity of 1650 m/s and a peak pressure of 3.6–5.2 MPa. For the same arrangement, only a decaying blast wave was observed, followed by particle combustion for atomized aluminum particles.

To study the propagation of Al–air detonation without confinement effects, a large-scale cloud was generated through a charge configuration arranged in an 18-m-long, 90 deg, V-shaped steel trough line, in which a PETN cord (21.3 g/m, 6.1 mm in diameter) was located at the bottom vertex covered by a layer of Al powder

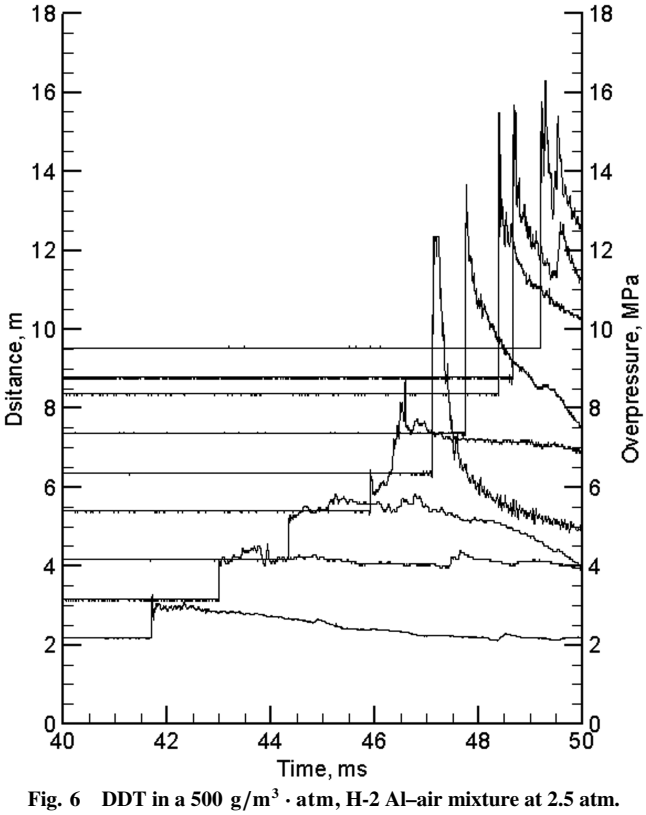

Fig. 6 DDT in a 500 g/m^3 · atm, H-2 Al–air mixture at 2.5 atm.

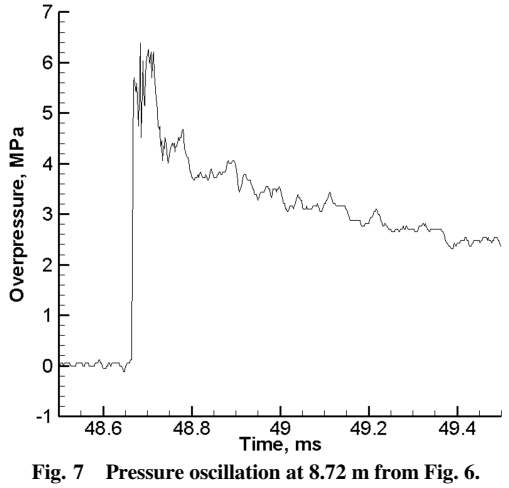

Fig. 7 Pressure oscillation at 8.72 m from Fig. 6.

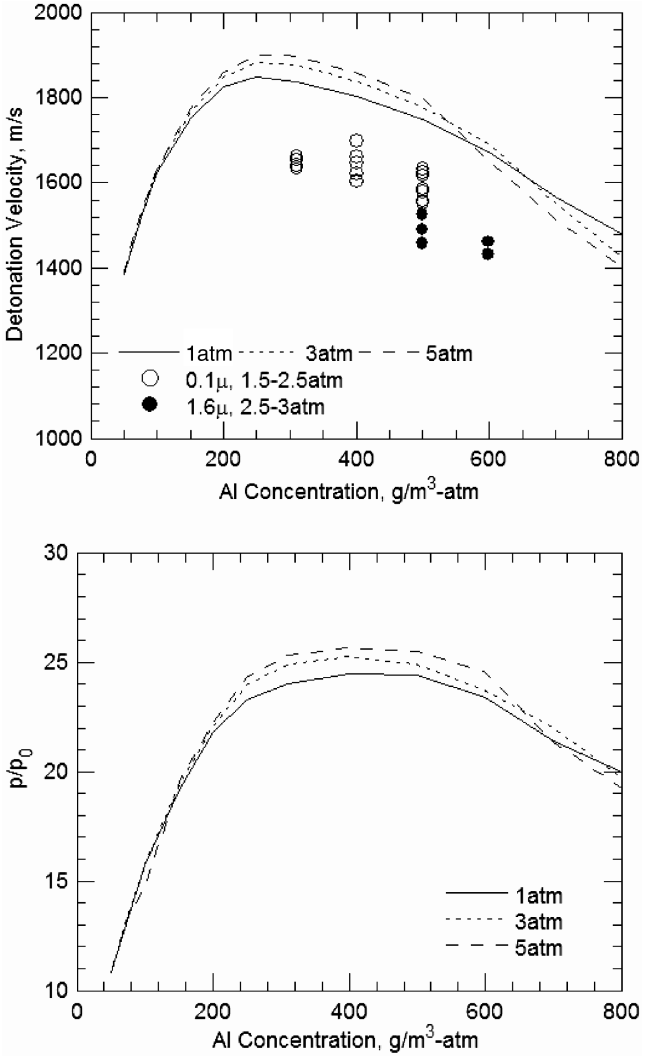

Fig. 8 Detonation properties in Al–air mixtures at various initial pressures: experimental detonation velocities (top, open and closed symbols) versus C-J values and C-J pressures (bottom).

[26]. Two types of Al particles were used: 47.6 kg H-2 atomized Al and 31.5 kg Silberline DF-1667 dedusted Al flakes, as shown in Fig. 1. Detonation of the PETN cord dispersed the Al powder in air to a 3-m-radius cross section and 18-m-long suspension at a given dispersal time. This resulted in an average Al concentration of 375 g/m^3 for H-2 atomized Al and 250 g/m^3 for flakes (or an equivalence ratio of 1.3 for H-2 Al and 0.9 for flakes based on the local air pressure of 91 kPa). The resultant Al–air cloud was initiated at one end using 8 kg C4 explosive located 1.5 m from the end as well as 1 m from the ground and the steel line. Experiments using an initiation explosive mass up to 5 kg were not able to achieve DDT within the H-2 Al–air cloud size. The wave phenomena were recorded using PCB pressure transducers located on the ground along the wave-propagation direction, 3 m from the C4 explosive for the first transducer and 2 m intervals for the rest.

Figure 9 shows an example of high-speed photographs for a DDT experiment in a flaked Al–air cloud, and Figs. 10 and 11 display the ground pressure histories along the propagation distance for a H-2 atomized Al and a flaked Al test, respectively. For the H-2 Al within a 4 m ground distance from C4, the shock velocity decays to 1300 m/s. The shock velocity further decays to 1050 m/s at 9 m, whereas Al combustion generates multiple compression waves behind the shock front during the propagation. At 13 m, abrupt DDT phenomena take place with a 5.5 MPa peak pressure and a pressure history featured with oscillations, a typical phenomenon related to the transverse waves. However, the cloud length is too short to determine the sustainability of the detonation wave.

For flaked Al shown in Fig. 11, the shock-front velocity is 1600 m/s at 4 m from the C4 location and decays to 1380 m/s at 7 m. At 11 m, the abrupt onset of overdriven detonation occurs with a peak pressure of 8.4 MPa. The 2 m averaged detonation velocity reaches a maximum value of 1533 m/s and remains 1460–1500 m/s in the remaining propagation. In the oscillating pressure histories recorded after 11 m, a transverse wave structure is distinguishable; it has a primary period of about 350–400 μs for the signal at 15 m, as displayed in Fig. 11. When multiplied by the propagation velocity, this oscillation period indicates a characteristic detonation size of 0.52–0.6 m. These experiments indicate that the 8 kg C4 is near the critical charge for direct initiation of flaked Al–air detonation, but is only marginal to directly initiate H-2 Al–air detonation. Note that without Al particles, the air-blast overpressure from the 8 kg C4 explosion decays rapidly to 0.186, 0.046, and 0.023 MPa at 5, 10, and 15 m, respectively.

IV. Aluminum Reaction Model

Khasainov and Veyssiere [4] applied a diffusion reaction model to Al–gas detonations; that is,

$$J_p = n_p \pi d_p^2 \rho_p \frac{dr_p}{dt} = -\frac{3\sigma_p}{t_b}(1 + 0.276 Re^{1/2} Pr^{1/3}) \ , \quad \text{if } T_p \geq T_{\text{ign}} \tag{1}$$

else $J_p = 0$. In Eq. (1), the particle burning time is

$$t_b = K d_{p0}^n / Y_{\text{oxi}}^\alpha \tag{2}$$

where J_p is the Al mass depletion rate in kg/m^3/s; n_p, T_p, d_p, r_p, σ_p, and ρ_p are the particle number density, temperature, diameter, radius, mass concentration and material density, respectively; Re is the Reynolds number based on the velocity difference between the two phases; Pr is the gas-phase Prandtl number; the parameters K, d_{p0}, Y_{oxi}, and T_{ign} are the rate coefficient, initial particle diameter, mass fraction of oxidizing gases, and particle ignition temperature, respectively; and $n = 2$ has been often used, which essentially assumes infinite chemical kinetics.

In fact, a diffusion-limited d^2 law can be derived for the particle burning time from the liquid-droplet combustion theory [5]:

$$t_b = \rho_p d_{p0}^2 / [8\rho D \ln(1 + \alpha Y_{\text{oxi}})] \sim \rho_p d_{p0}^2 / 8\rho D \alpha Y_{\text{oxi}} \tag{3}$$

where ρD, and Y_{oxi} represent the gas density–diffusivity product at the particle surface and oxygen mass fraction in air, respectively. The d^2 law expressed in Eq. (3) is independent of temperature and pressure and is obtained for a particle located in a quiescent flow, assuming infinite gas-phase reactions. It is inappropriate when used for convective flow, elevated pressures, and small aluminum particles, as commented in the Introduction of this paper. Thus, the term including the Reynolds number was introduced in Eq. (1), presumably to consider the convective flow influence. The model has been widely used in computational fluid dynamics codes to model the propagation of detonation, assuming an ignition temperature (933–1350 K) much below the oxide melting point [2,4,27–29]. Apart from diffusion models, Arrhenius kinetics models have also been applied recently to Al–gas detonations [30,31].

As observed in the experiments described in the previous sections, Al–air detonation strongly depends on initial pressure; the abrupt DDT, both in tubes and unconfined clouds, indicates a highly nonlinear dependence on temperature. These facts suggest a dependence of detonation initiation and DDT on chemical kinetics. On the other hand, Al–air detonation exhibits a weak transverse wave structure indicated by the weak pressure oscillation behind the shock front. This weak transverse wave structure could suggest a weaker functional dependence than the highly nonlinear Arrhenius kinetics for some late-time Al combustion that supports the transverse wave. The weak transverse wave structure was also observed previously for flaked Al–air detonation in a 0.3-m-diam, 42-m-long tube, in contrast to the strong transverse wave structure obtained for

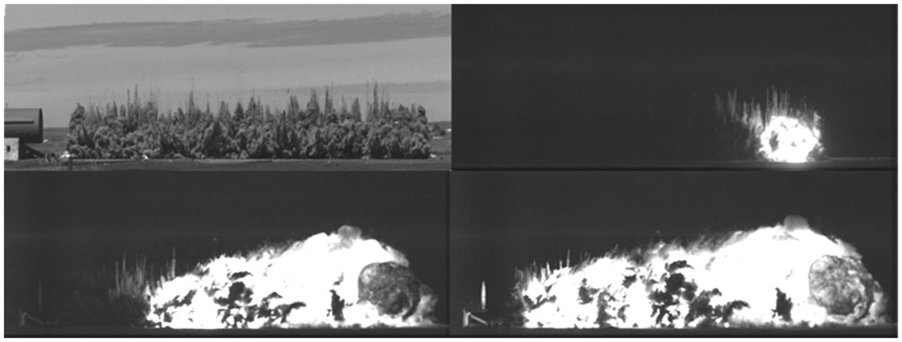

Fig. 9 Detonation in unconfined flaked Al–air: Al suspension (top left), initiation (top right), detonation propagation (bottom left and right).

cornstarch-particle–air mixtures using the same tube (see Figs. 12 and 13 from [22]). This observation is consistent with the experimental results reported in the current paper and further supports the postulation of a weaker nonlinear functional dependence of some Al reaction with a degree of condensed Al oxides in the detonation products, whereas the reaction of cornstarch more closely follows the Arrhenius gas-phase kinetics, due to a high-volatile content, and results in mainly gaseous detonation products.

In accordance with these experimental facts, a kinetics-diffusion hybrid reaction model is proposed by the authors in the form [26]

$$J_p = -n_p \pi d_p^2 k_p = -n_p \pi d_p^2 \frac{\nu_p W_p}{\nu_{\text{oxi}} W_{\text{oxi}}} k \tag{4}$$

$$k = k_d (C_{\text{oxi}} - C_{\text{oxi},s}) \quad \text{or} \quad k = k_s C_{\text{oxi},s} = C_{\text{oxi},s} k_0 e^{-E/RT_s} \tag{5}$$

where k_p and k are the mass depletion rate (equaling the mass flux) of the particle and oxidizing gas at the particle surface in the r direction, respectively; k_d and k_s are the rate coefficient for diffusion and surface chemical reaction, respectively; and W, ν, C_{oxi}, and $C_{\text{oxi},s}$ denote the molecular weight, stoichiometric coefficient, oxidizing gas mole concentration, and its particle surface value, respectively. $T_s = (T_g + T_p)/2$ is assumed to be the particle surface temperature.

From Eq. (5), one obtains the hybrid model by making the diffusion and surface chemical-reaction expressions equal:

$$k = \frac{k_d k_s}{k_d + k_s} C_{\text{oxi}} \tag{6}$$

The diffusion rate coefficient k_d can be obtained by inserting the diffusion model (1) and (2) ($a = 1$ is assumed for simplicity) into Eqs. (4) and (6):

$$k_d = \frac{\nu_{\text{oxi}} W_{\text{oxi}}}{\nu_p W_p} \frac{\rho_p d_p}{2 C_{\text{total}} K d_{p0}^2} (1 + 0.276 Re^{1/2} Pr^{1/3}) \tag{7}$$

where C_{total} is the mole concentration of total gases. Equation (5) yields the surface reaction rate coefficient:

$$k_s = k_0 e^{-E/RT_s} \tag{8}$$

Thus, Eqs. (4) and (6–8) form the hybrid reaction model, which depends on temperature, pressure via oxidizing gas concentration, and particle size (inherent from the diffusion rate) and does not need a presumed particle ignition temperature. The model becomes surface-kinetics-limited ($k \to k_s$) when $k_s/k_d \ll 1$, and diffusion-limited ($k \to k_d$) when $k_s/k_d \gg 1$.

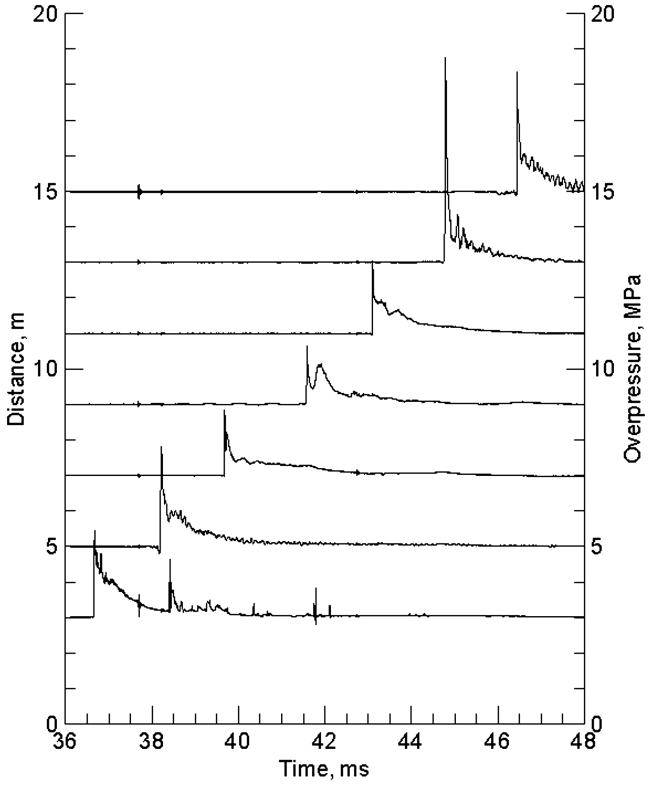

Fig. 10 Unconfined H-2 Al–air DDT.

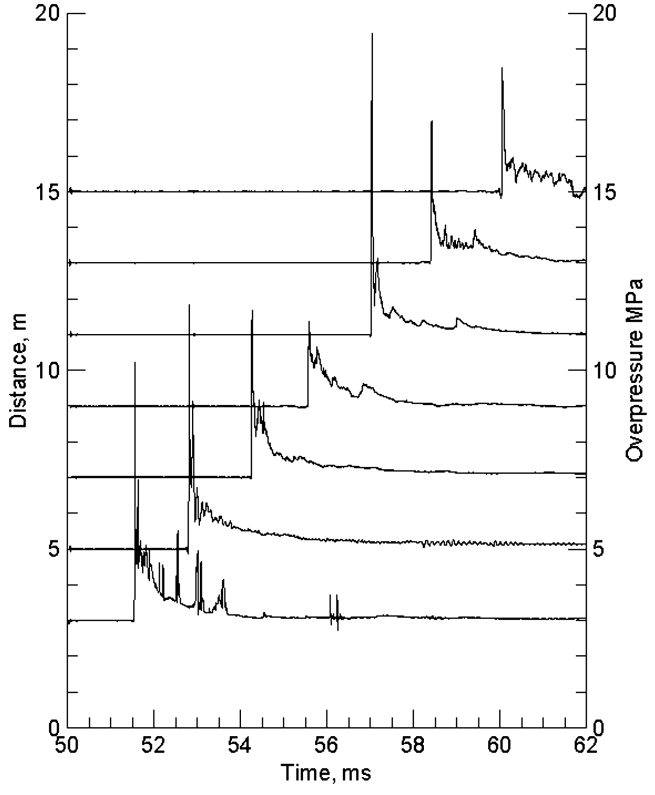

Fig. 11 Unconfined flaked Al–air DDT.

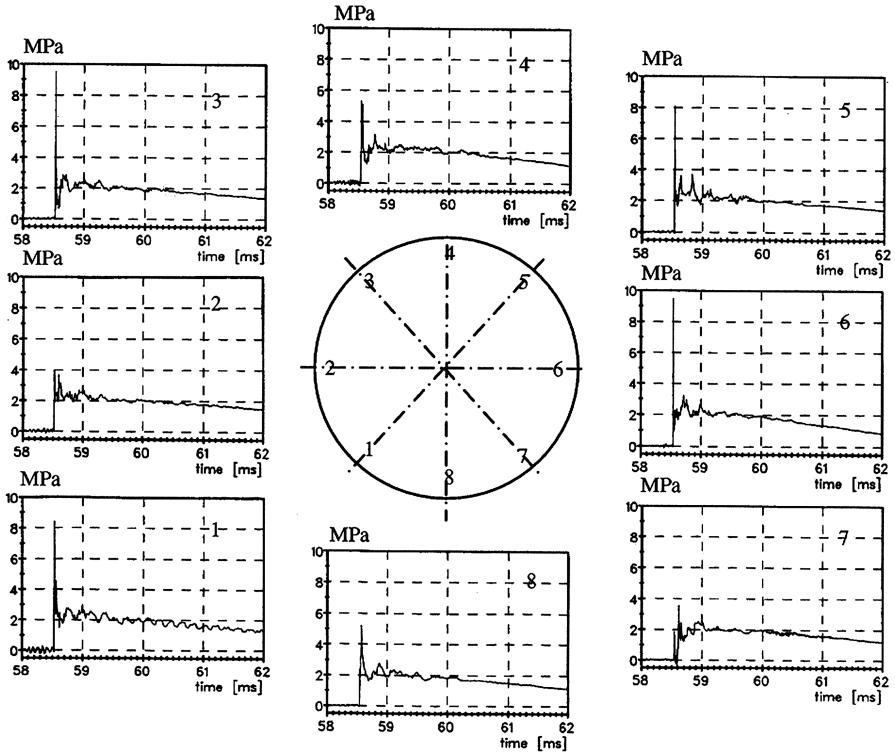

Fig. 12 Pressure profiles on a circumference at $x = 24.8$ m of a 0.3-m-i.d., 42-m-long tube filled with a 500 g/m^3 flaked aluminum–air mixture at 1 bar [22].

Figure 14 illustrates a comparison between the diffusion, kinetic, and resulting hybrid reaction rates from Eqs. (6–8) as a function of particle size and temperature, where $K = 4 \times 10^6$ s/m^2, $k_0 =$ 1200 kg · m/mol · s, and $E = 71.1$ kJ/mol. Without involving any shock process or conservation equations of the two-phase-flow, momentum equilibrium ($u_g = u_p$) and lack of particle reaction ($d_p = d_{p0}$) are simply assumed to enable calculations using Eqs. (6–8) alone. Although the momentum-equilibrium assumption is inappropriate for large particle sizes in general, the comparison does elucidate some basic behavior of the model. As shown in Fig. 14, the line for the kinetic rate is independent of particle size, whereas the diffusion rate decreases as the initial particle size increases. Thus, the overall hybrid reaction rate depends on particle size between a chemical kinetics limit ($d_{p0} \sim 1$ μm at $T_s = 933$ K

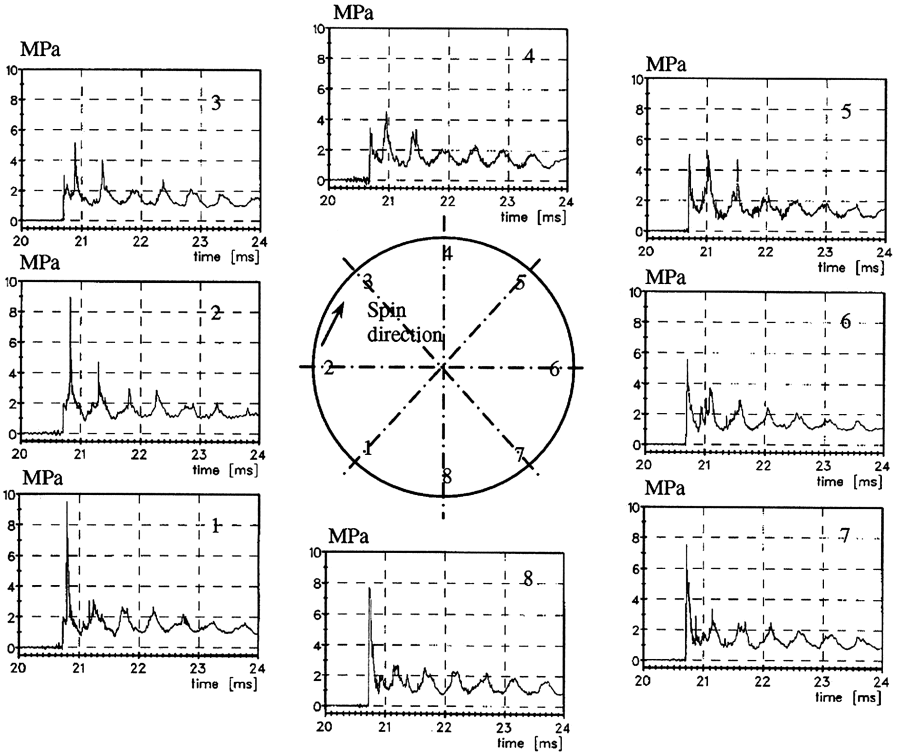

Fig. 13 Pressure profiles on a circumference at $x = 24.8$ m of a 0.3-m-i.d., 42-m-long tube filled with a 400 g/m^3, 10 μm cornstarch–air mixture at 1 bar [22].

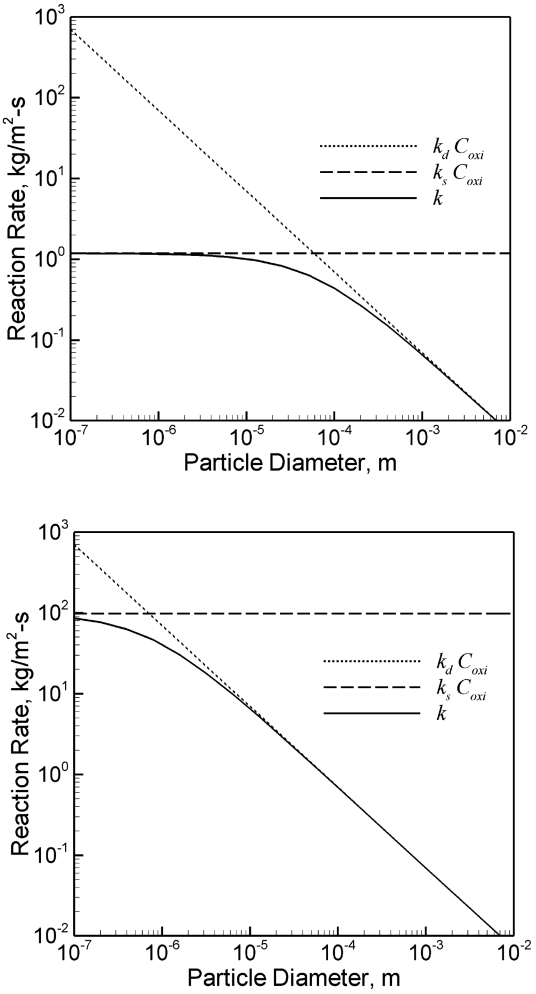

Fig. 14 Reaction rates versus initial particle size: $T_s = 933$ K (top) and $T_s = 1800$ K (bottom).

and $d_{p0} < 0.1$ μm at $T_s = 1800$ K) and a diffusion limit ($d_{p0} \sim 1$ mm at $T_s = 933$ K and $d_{p0} \sim 10$ μm at $T_s = 1800$ K). With an increase in temperature, the value at the point of $k_s/k_d = 1$ increases, and therefore the limits shift toward the side of smaller particles. In general, the model predicts a more dominant reaction by the surface kinetics at low temperatures and small particles, whereas the diffusion reaction controls more at high temperatures and large particles.

V. Numerical Results and Discussion

The hybrid reaction model is implemented in the Chinook code (Martec, Ltd.), a second-order unsteady Eulerian multiphase fluid dynamics code for which the governing equations can be found in [32,33] and are described in the Appendix. In the multiphase fluid dynamics model, the solid phase and gas phase have been treated as two separate flows (different velocity and temperature) and their mass, momentum, and energy are exchanged through the source terms. Noting that Al_2O_3 generally does not exist as a gas and its latent heat of melting is very small, a single-step global reaction of aluminum and oxygen was simply assumed to form solid Al_2O_3 with a heat of reaction of 838 kJ/mol. The species involved in this global reaction are Al(s), Al(l), Al(g), O_2, N_2, and $Al_2O_3(s)$. The Al latent heats of melting and evaporation were 10.7 and 290 kJ/mol, respectively. For the Al–gas detonation problem involved, the solid flow can be assumed to be dilute and the particle material is incompressible. The ideal-gas equation of state was employed for the air and detonation-product gas, with the temperature-dependent heat capacities and specific heat ratio based on NASA CEA program temperature fitting [34]. The HLLC (Harten–Lax–van Leer with contact correction) approximate Riemann solver was extended to solve the fluxes for both gas and discrete solid flow [35]. In the following one-dimensional calculations, $K = 4 \times 10^6$ s/m^2, $k_0 = 1200$ kg $\cdot$ m/mol $\cdot$ s, and $E = 71.1$ kJ/mol were used. Simulations were conducted for the rich 2 μm Al–air mixture at $\sigma_p = 1250$ g/m^3 and an initial pressure of $p_0 = 2.5$ atm, the same initial conditions as the experiment displayed in Fig. 6. To illustrate the intrinsic mechanism for the multiphase Al–air detonation, the source terms for wall losses were not included in the calculations, and therefore the results remain as a theoretical description without taking into account the deficit of detonation velocity observed in the experiments.

Figure 15 shows one-dimensional simulation results of DDT using a 6.13 kJ initiation energy within a 1 mm numerical cell ($p = 8.56$ p_0, $T_g = 2567$ K, and $T_p = 300$ K). The results clearly show that after an ignition delay behind the shock front, a local Al–air explosion leads to the abrupt onset of detonation. Thereafter, the overdriven detonation relaxes toward a detonation, with a 1758 m/s detonation velocity and 37.58 p_0 peak pressure at $x = 19$ m (note that the detonation is still relaxing). During the early DDT process, $k_s/k_d < 1$ holds behind the shock front in an induction stage that leads to local explosion, thus indicating a kinetics-limited reaction in the induction stage (Fig. 16). As the local explosion develops, the particle temperature rapidly increases and hence results in a rapid decrease in induction zone and an increase in k_s/k_d. Once the detonation forms, $k_s/k_d > 1$ holds after a short kinetics induction time behind the shock, thus showing a diffusion-limited reaction for most of the Al mass depletion. The process is in agreement with the experimental results shown in Fig. 6, and therefore the hybrid model properly describes the detonation initiation and abrupt DDT. Calculations using the diffusion model (1) and (2) showed that abrupt DDT via autoexplosion centers cannot be obtained under the same initial conditions; instead, there is a smooth progressive acceleration to detonation that conflicts with the experimental observation.

Figure 17 displays the diffusion, kinetic, and resulting hybrid reaction rates at the specific von Neumann shocked state of the C-J detonation front ($D = 1745$ m/s, $u_g = 1396$ m/s, $T_g = 1748$ K, $u_p = 0$, $T_p = 300$ K, $\rho_g = 14.66$ kg/m^3, and $p_g = 29.05p0$ at $p_0 = 2.5$ atm). It clearly shows that for 2 μm Al particles, $k_s/k_d < 1$ holds and the surface kinetic reaction is dominant at the von Neumann state, thus indicating the existence of a kinetic induction zone at the detonation front during its propagation.

Because the low activation energy and long diffusion-combustion time result in a low induction/reaction length ratio, detonation becomes steady after a sufficient propagation distance. Hence, a steady one-dimensional Zeldovich–Neumann–Döring (ZND) detonation structure can be obtained by the long-time asymptotic unsteady solution. This long-time asymptotic solution was achieved using an incoming flow entering a 0.1 mm grid resolution

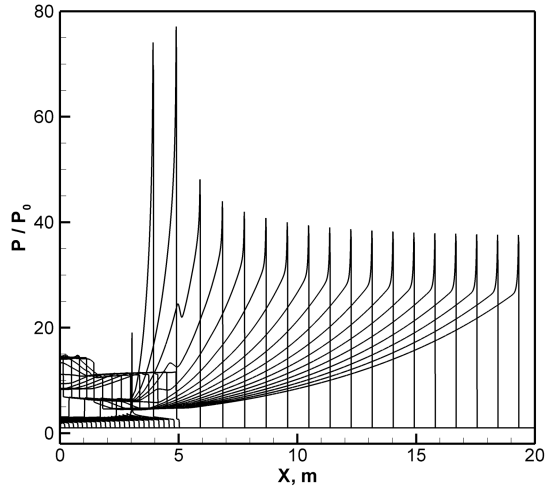

Fig. 15 DDT pressures using the hybrid model.

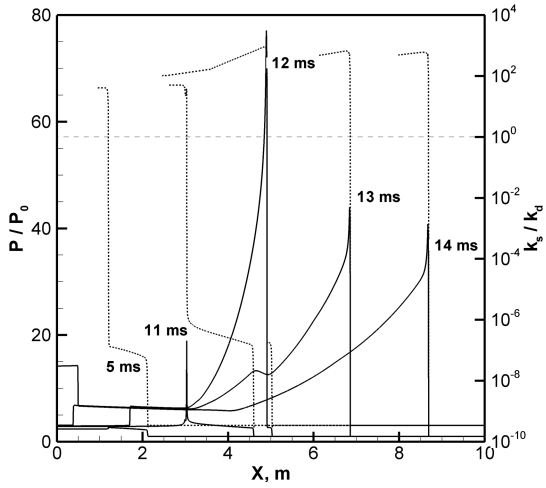

Fig. 16 The early process in Fig. 15: p/p_0 (solid line) and k_s/k_d (dotted line).

computational domain, in which the incoming flow has the same initial conditions as described previously, but with a flow velocity equal to the C-J detonation velocity.

The obtained ZND detonation structure, shown in Figs. 18 and 19, starts at the Hugoniot jump of a shock front, followed by a short induction and long reaction zone, successively, and is terminated at the equilibrium sonic locus in which the equilibrium C-J condition is satisfied. In the short induction stage (see Fig. 18), although the particles are heated through convective heat transfer from the shocked gas, the drag compression continuously increases the gas pressure, temperature, and Al concentrations. Significant heat release of the particles into the gas takes place in the following reaction stage, and the resultant gas expansion causes the pressure to decrease toward 23 p_0 when the flow moves toward the sonic locus (Fig. 19). The expansion of the high-pressure gases provides the work to sustain the propagation of the shock front, which in turn supports the momentum and heat transfer between the two phases and the ignition of particles behind the shock front. Much before the sonic locus, the two-phase velocity and temperature equilibrium ($u = u_g = u_p$ and $T = T_g = T_p$) are reached, and the reaction proceeds thereafter in a nearly phase-equilibrated flow. Hence, the C-J equilibrium detonation solution with respect to the full equilibrium (both chemistry and phase) sound speed a_e is achieved with $D - u = a_e$. In contrast, a condition popularly used in the so-called two-phase ZND detonation model in the literature [2,4], the generalized C-J condition at the phase-frozen sound speed ($D - u_g = a_g$), failed in this example. In fact, the phase-equilibrated flow is still subsonic with respect to the phase-frozen sonic speed a_g as the C-J equilibrium condition is achieved.

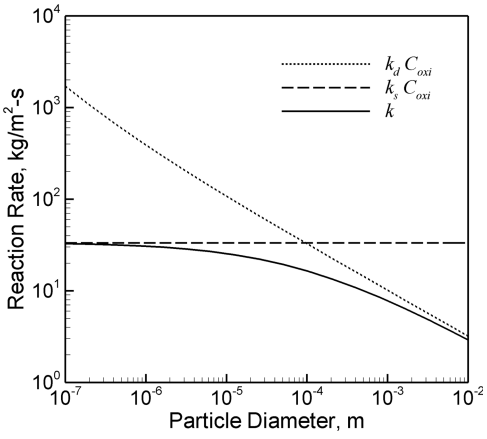

Fig. 17 Reaction rates versus initial particle size at the von Neumann shocked state.

In general, the solid-particle–gas-flow ZND structure has several significant differences from a ZND structure for homogeneous gas detonation [33]. First, the shock-front pressure (i.e., the von Neumann spike) in a gaseous detonation corresponds to the maximum pressure, whereas the maximum pressure for a reactive particles-oxidizing gas detonation wave may be found behind the shock front at a point at which the combustion expansion balances the drag compression (see Fig. 18, in which the von Neumann spike equals 29.05 p_0). Second, the equivalence ratio of the particle–gas mixture behind the shock front does not remain the same as the initial value ahead of the shock front. The velocity relaxation time lag, in which the particles are accelerated toward the gas velocity before burning, results in a nonuniform equivalence ratio field behind the shock, with a shift from the initial equivalence ratio of fuel particles to oxidizing gas toward a leaner value. This is clearly indicated in the mass fraction of Al in the mixture behind the shock front in Fig. 18, in which a preshock initial Al mass fraction is 0.3 (not shown in Fig. 18). Third, the ZND structure is also characterized by melting and evaporation phase changes, as shown in Figs. 18 and 19. In this example, a constant particle temperature was assumed during the phase change from liquid Al to vapor, whereas the internal energy was increased to overcome the threshold of a large Al latent heat of evaporation. The melting and evaporation model can be further improved, for instance, by introducing the Clausius–Clapeyron equation. As the evaporation proceeds, the gas pressure and density show a clear second peak, partially due to the rich aluminum in the mixture.

The preceding simulations assume that the condensed Al and Al_2O_3 in the detonation products are incompressible without contribution to gas pressure. When Al_2O_3 was included in a gas phase in the detonation products, the simulation showed that the detonation velocity and peak pressure were increased to 2290 m/s and 61 p_0, respectively. This is obvious, because the work supporting the shock propagation is done directly by the expansion of the gaseous detonation products.

The current global Al reaction model addresses the dual features of chemical kinetics and diffusion-limited reaction under detonation conditions. Improvement to the hybrid model would need to further examine other main factors that influence the Al reaction. For instance, the assumption of the solid Al_2O_3 products is over-simplified and might cause the overprediction of the temperature in Fig. 19. The achieved detonation temperature of about 5000 K considerably exceeds the Al_2O_3 melting point (~2300 K) and decomposition point (~3253 K). Borisov et al. [2] and Benkiewicz and Hayashi [28] proposed a model of endothermic decomposition of Al_2O_3 into gaseous aluminum suboxides as the temperature

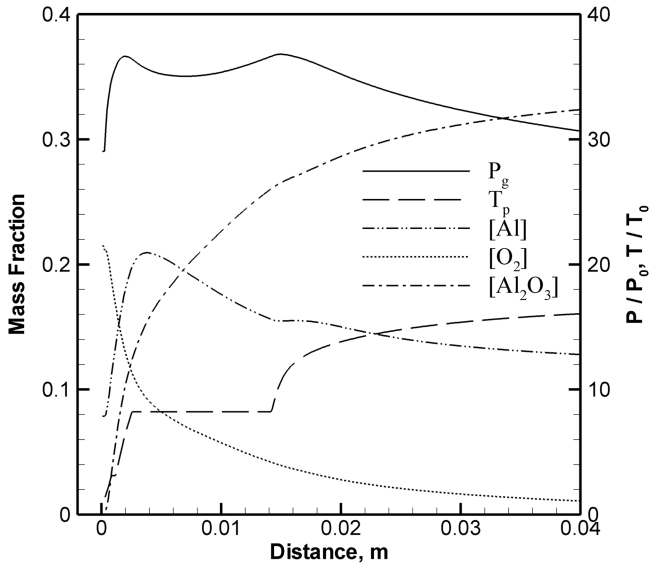

Fig. 18 Early phase of the 1-D two-phase ZND detonation structure.

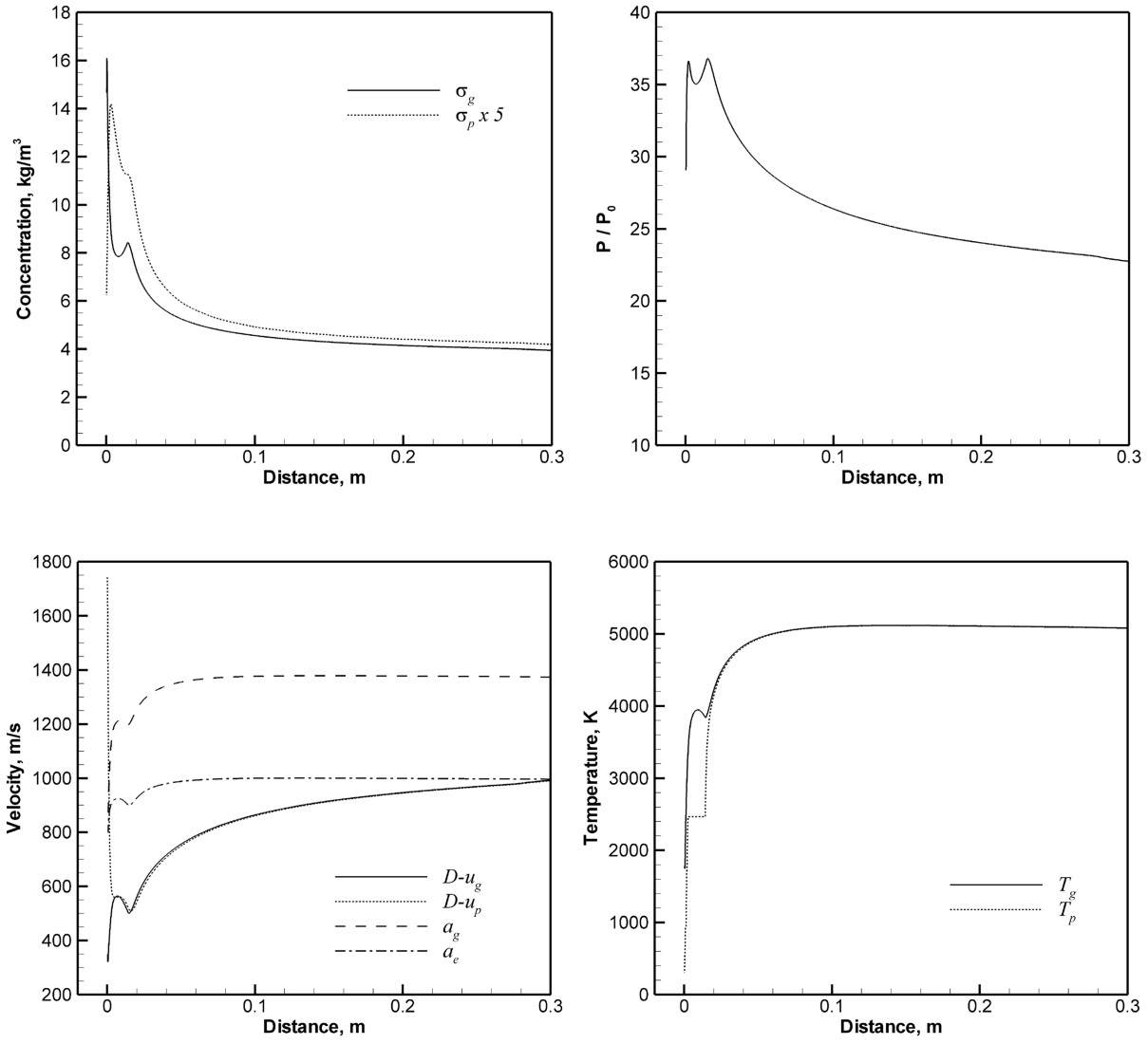

Fig. 19 1-D two-phase ZND detonation structure.

reaches the decomposition point, thus controlling the temperature growth below a certain value. In reality, gaseous Al oxides such as AlO have been experimentally found in the detonation products, and their expansion work should be partially responsible for sustaining the detonation propagation in the stoichiometric Al–oxygen mixture as observed in the early experiment of Strauss [36]. Thus, the model should be extended to include two irreversible Al reactions with the second reaction being endothermic:

$$\mathrm{Al} + 4/3\mathrm{O_2} \Rightarrow 1/2\mathrm{Al_2O_3} - 838\ \mathrm{kJ/mol} \tag{9}$$

$$\mathrm{Al} + 1/2\mathrm{O_2} \Rightarrow \mathrm{AlO} + 91\ \mathrm{kJ/mol} \tag{10}$$

Note that the two irreversible exothermic–endothermic reactions with $|q_1| > |q_2|$ and mole decrement due to a large quantity of condensed Al oxide may lead to a pathological detonation when the products' Hugoniot shifts to the left of the reactants' Hugoniot [37]. Apart from more detailed Al reaction schemes under shock conditions, more accurate models will also require understanding of the morphology of the Al particles, including oxide-layer damage behind the shock front.

To justify the qualitative physical phenomena described by the numerical simulation, one-dimensional unsteady calculations were conducted using two mesh resolutions of 1 and 0.1 mm. Because the corresponding nondimensional grid resolution is approximately $1/300$ and $1/3000$ with respect to the reaction length of the detonation zone (0.307 m using the 0.1 mm mesh), the observed detonation phenomena are qualitatively similar. The detonation-front peak pressure and the reaction length are 36.33 p_0 and 0.295 m for the 1 mm mesh and 36.63 p_0 and 0.307 m for the 0.1 mm mesh, thus indicating a grid convergence of the solution. Although the 1 mm mesh approximately describes the main detonation phenomena, it does not resolve the melting and the kinetic induction, and therefore the abrupt DDT is not sufficiently resolved. Hence, the current numerical results remain as a qualitative description of the aluminum reaction mechanism associated with the DDT. Finer grid resolution and systematic grid convergence studies will be considered in the future toward more qualitative modeling in comparison with experiments.

To further examine the suitability of the hybrid reaction model for the Al detonation, long-time two-dimensional simulations were performed with a 1 mm numerical cell size on a domain 1 m wide by 4.75 m long. A hot-spot region spanning the width of the domain with a singular instability was introduced at the beginning of the calculation to initiate the detonation and transverse wave structure. The calculations were run for 50–70 ms, equivalent to the detonation running 90–120 m. The same Al–air mixture initial conditions and parameters of the hybrid reaction model as those used in the one-dimensional computations were employed here, except for the variation of the activation energy only.

Figure 20 presents the numerical shadowgraph from the gas-pressure data. In these instantaneous snapshots, the transverse wave structure is visible, and the lightest and darkest regions denote

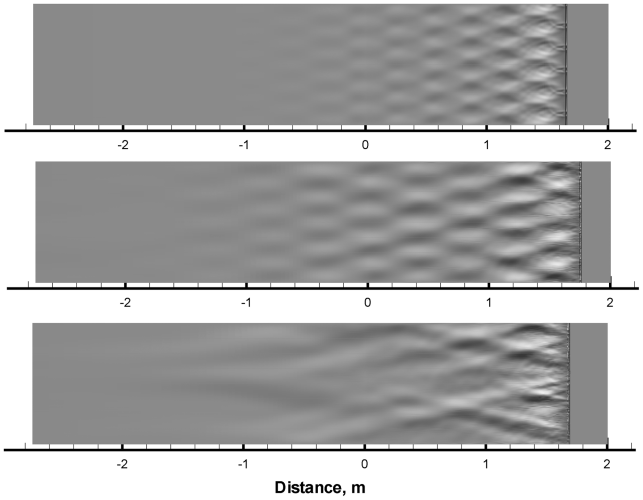

Fig. 20 Numerical shadowgraph from the pressure data of 2-D detonation simulations: $E = 71.1$ kJ/mol (top), $E = 95.5$ kJ/mol (middle) and $E = 120$ kJ/mol (bottom).

regions of highest gradient. As the activation energy increases, detonation instability indicated by the cell irregularity increases, with an increase in detonation cell width from 0.18, 0.22, to 0.28 m, respectively. For all activation energies used in Fig. 20, the transverse waves behind the leading shock front are generally weak and degenerate fairly fast in the rear flow, and local pressure oscillation histories have been found to be relatively smooth. This is attributed to the slower diffusion-dominated combustion of the majority of Al mass after the kinetic induction and a considerable amount of condensed Al oxide (without direct contribution to gas pressure) in the mole decrement detonation products. These factors tend to reduce the rapid rate of expansion work of the detonation products required to maintain the strength of the transverse wave in the two-phase rear flow.

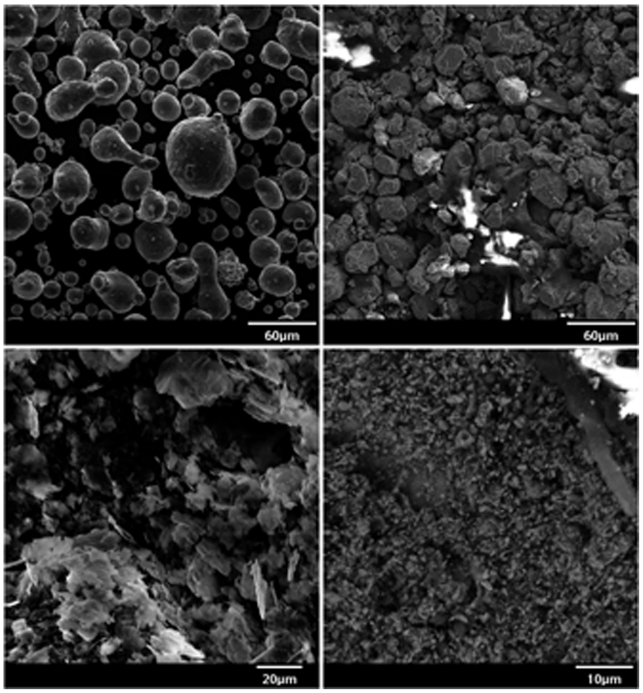

Fig. 21 Aluminum-particle SEM samples before and after flyer-plate impact that generates a 13 GPa incident shock into the particles saturated with inert liquid heptane (no oxygen): Valimet, Inc., H-30 atomized aluminum particles before (left) and after (right) a test (top) and Silberline DF-1667 dedusted Al flakes before (left) and after (right) a test (bottom). Courtesy of Yoshinaka et al. [38].

The instability of micrometric Al–air detonation with a weak transverse wave structure is in agreement with the experimental observations presented previously. This is in contrast to the simulation results by Benkiewicz and Hayashi [28] using the diffusion model alone in Al–oxygen mixtures, in which a strong transverse wave structure persists for a long period in the rear flow behind the detonation front. In the present work, calculations using the diffusion model alone failed to predict a change in the detonation instability route, leading to the irregularity of the detonation cells. Although the weak and irregular transverse wave structure has been obtained currently by applying the hybrid reaction model to the monosized Al-particle suspension, one would expect that simulations using a multisized particle distribution of the tested H-2 Al, as shown in Fig. 1, may result in a more multiple-length-scale wave structure, due to multiple time-scale reaction rates of various particle sizes. In a recent work, Fedorov and Khmel [31] conducted numerical calculations using two Al-particle sizes in a suspension with an Arrhenius kinetic model that was overconstrained by an artificial ignition temperature. They reported a persistent transverse wave structure in the detonation rear flow for a monosuspension of each particle size, but attenuation and degeneration of the transverse wave structure resulted by mixing two particle sizes to a considerable mass fraction of each. As referred to earlier in Sec. IV, whereas the Al–air detonation displayed a weak transverse wave structure, the cornstarch–air detonation exhibited a strong transverse wave structure in the same tube and test conditions [22]. Because both the Al particles and cornstarch tested had a multiple-size particle distribution, one of the more reasonable explanations would be that the reaction of Al particles is subject to a degree of slower diffusion-limited reaction with a large amount of condensed Al oxide in the mole decrement detonation products, whereas the reaction of cornstarch mostly follows the highly nonlinear Arrhenius gas-phase kinetics, due to a high-volatile content, and results in primarily gaseous detonation products.

When compared with the real-world three-dimensional experiments, an activation energy $E = 95.5$–120 kJ/mol would be suggested by the hybrid Al reaction model, in agreement with the experimental DDT distance and the pressure oscillation period observed in Figs. 6 and 7.

VI. Conclusions

Experimental observations clearly indicate that the detonation of aluminum-particle–air mixtures is affected by the magnitude of initial pressure for a particle-size range from 100 nm to 1.6 μm (mean diameter by number). It was found in an 80-mm-diam tube that the 100 nm Al–air detonation can be initiated at 1 atm initial pressure, whereas the 1.6 μm atomized Al–air detonation only becomes possible when the initial pressure is increased to 2.5 atm. The observed DDT process clearly exhibits an abrupt nature via local explosion events. An increase in initial pressure results in an increase in detonability and a decrease in DDT distance. The abrupt nature of DDT is further confirmed in the large, unconfined, Al–air cloud experiments without the tube wall restraint. In both the tube and unconfined cloud cases, the detonation for the micrometric Al–air manifests itself in a weak transverse wave structure, as indicated by the small-amplitude oscillation that rapidly degenerates behind the shock front in the pressure histories. The characteristic detonation cell sizes obtained in the tube ($\sim$0.23 m at 2.5 atm) and for the unconfined cloud (0.52–0.6 m near 1 atm) indicate a nearly inversely proportional relationship between the cell size and initial pressure.

The strong dependence of nanometric and micrometric Al–air detonation sensitivity on initial pressure and the highly nonlinear abrupt DDT nature suggest that the Al reaction mechanism of these detonation waves must depend on chemical kinetics. Aluminum combustion models based on the pressure- and temperature-independent fuel-droplet diffusion theory alone appear to be insufficient in describing Al–air detonation initiation, transition, and structure in respect to unsteady dynamic behaviors. On the other hand, the weak

transverse wave structure of the Al–air detonation indicates some functional dependence that is weaker than the Arrhenius kinetic behavior and is likely associated with some slower diffusion combustion of Al mass in the later time and a large amount of condensed Al oxide in the mole decrement detonation products. A surface kinetic oxidation and diffusion hybrid reaction model was therefore suggested in which the Arrhenius kinetics are mainly correlated to the Al ignition behavior, and the late Al combustion is more subject to the diffusion-limited reaction. The one-dimensional and two-dimensional unsteady two-phase fluid dynamics modeling demonstrated the success of the hybrid reaction model, capable of capturing both the kinetics-dependent transient processes of detonation initiation, abrupt DDT and the detonation instability, and the diffusion-limited combustion of Al in the long reaction zone supporting the weak transverse wave structure.

Although the current hybrid Al reaction model addresses the dual features of chemical kinetics and diffusion-limited reaction under detonation conditions, improvement to the model will need to further examine other main factors that influence the Al reaction. The exothermic global reaction model with the assumption of condensed Al_2O_3 products alone should be extended to at least two Al reactions, with the second reaction being endothermic, which generates gas-phase AlO that contributes to the expansion work of the gaseous detonation products and improves the prediction of detonation temperature. The parameters for the Al hybrid reaction model will be further correlated with the fundamental shock ignition-delay data, and the model will be tested in terms of describing the kinetics-dependent processes of detonation failure and quenching.

One of the key phenomena unresolved for the Al reaction mechanism under detonation conditions is possibly the damage to the aluminum oxide coating due to mechanical and thermal interaction of the particles with the shock wave. The extent to which the bare Al is exposed through oxide-coating removal or cracking will influence the aluminum ignition and reaction process. Recent flyer-plate impact experiments simulating detonation in condensed phase matter (with an incident shock pressure of 13 GPa) showed that the atomized particles were subjected to severe surface damage and breakup to exposed fresh bare aluminum, whereas aluminum flakes were completely broken into nanometric particles (see Fig. 21 from [38]). This helped to understand why aluminum reacts much faster under high-pressure condensed detonation conditions. There have been no direct experiments simulating the Al–gas detonation conditions to recover and analyze the Al-particle morphology subjected to a shock interaction. More accurate reaction models will require understanding of the morphology of the Al particles and the oxide-layer damage behind the shock front as well as the detailed Al reaction schemes under shock conditions.

Appendix: Two-Phase Fluid Dynamics Equations

For the supersonic detonation flow involved, the viscosity and conductivity in the fluid as well as particle gravities are not considered. From the control volume analysis, the one-dimensional conservation equations can be derived as listed next in the laboratory coordinate frame [32,33].

Solid-phase mass:

$$\frac{\partial \sigma_p}{\partial t} + \frac{\partial}{\partial x}(\sigma_p u_p) = J_p \tag{A1}$$

Solid-phase momentum:

$$\frac{\partial}{\partial t}(\sigma_p u_p) + \frac{\partial}{\partial x}(\sigma_p u_p^2 + p_p) = u_p J_p + f_p \tag{A2}$$

Solid-phase energy:

$$\frac{\partial}{\partial t}[\sigma_p(e_p + u_p^2/2)] + \frac{\partial}{\partial x}[\sigma_p u_p(e_p + u_p^2/2 + p_p/\sigma_p)] = (e_p + u_p^2/2)J_p + u_p f_p + Q_p \tag{A3}$$

Solid-phase number density:

$$\frac{\partial n_p}{\partial t} + \frac{\partial}{\partial x}(n_p u_p) = \Psi_p \tag{A4}$$

Fluid-phase mass:

$$\frac{\partial \phi_g \rho_g}{\partial t} + \frac{\partial}{\partial x}(\phi_g \rho_g u_g) = -J_p \tag{A5}$$

Fluid-phase momentum:

$$\frac{\partial}{\partial}(\phi_g \rho_g u_g) + \frac{\partial}{\partial x}(\phi_g \rho_g u_g^2 + \phi_g p_g) = -u_p J_p - f_p \tag{A6}$$

Fluid-phase energy:

$$\frac{\partial}{\partial t}[\phi_g \rho_g(e_g + u_g^2/2)] + \frac{\partial}{\partial x}[\phi_g \rho_g u_g(e_g + u_g^2/2 + p_g/\rho_g)] = -(e_p + u_p^2/2 + q_p)J_p - u_p f_p - Q_p \tag{A7}$$

Fluid-phase species:

$$\frac{\partial}{\partial t}(\phi_g \rho_g Y_j) + \frac{d}{dx}(\phi_g \rho_g u_g Y_j) = w_j, \qquad j = 1, \ldots, M \tag{A8}$$

where

$$\phi_g + \phi_p = 1 \tag{A9}$$

$$\sigma_p = \phi_p \rho_p \tag{A10}$$

$$n_p = \frac{6\phi_p}{\pi d_p^3} = \frac{6\sigma_p}{\pi \rho_p d_p^3} \tag{A11}$$

$$w_{O_2} = J_p \frac{\nu_{O_2} W_{O_2}}{\nu_{Al} W_{Al}}, \qquad w_{Al_2O_3} = -J_p \frac{\nu_{Al_2O_3} W_{Al_2O_3}}{\nu_{Al} W_{Al}} \tag{A12}$$

For the Al–gas detonation involved in this paper, the solid flow is dilute and the particle material can be assumed to be incompressible. Thus, $\phi_p = 0$, $p_p = 0$, and $\rho_p =$ constant. The particle temperature is computed from the internal energy:

$$T_p = \begin{cases} e_p/c_{pv} & \text{for } e_p \le c_{pv}T_{pm} \\ T_{pm} & \text{for } c_{pv}T_{pm} < e_p \le c_{pv}T_{pm} + L_m \\ (e_p - L_m)/c_{pv} & \text{for } c_{pv}T_{pm} + L_m < e_p \le c_{pv}T_{pb} + L_m \\ T_{pb} & \text{for } c_{pv}T_{pb} + L_m < e_p \le c_{pv}T_{pb} + L_m + L_b \\ (e_p - L_m - L_b)/c_{pv} & \text{for } e_p > c_{pv}T_{pb} + L_m + L_b \end{cases} \tag{A13}$$

The ideal-gas equation of state was employed for the air and detonation-product gas, with the temperature-dependent heat capacities and specific heat ratio based on NASA CEA temperature fitting [34].

The rate of mass transfer J_p is expressed in Eqs. (4) and (6–8) in Sec. IV. The drag f_p is formally expressed by

$$f_p = n_p \frac{\pi d_p^2}{4} C_d \rho_g (u_g - u_p)|u_g - u_p|/2 \tag{A14}$$

$$C_d = \frac{24}{Re}\left(1 + \frac{1}{6}Re^{2/3}\right) \tag{A15}$$

Assuming that the radiation heat transfer and the Biot number are small (ratio of convective heat transfer to the particle to conductive heat transfer within the particle), a uniform temperature within the particle is quickly established, and the rate of heat transfer Q_p to convection can be written by

$$Q_p = n_p \pi d_p Nu \lambda_g (T_g - T_p) \tag{A16}$$

$$Nu = 2 + 0.459 Re^{0.55} Pr^{0.33} \tag{A17}$$

Finally, the particle number conservation is simply assumed in this problem (i.e., $\Psi_p = 0$). The preceding one-dimensional governing equations can be straightly extended to the two-dimensional form.

References

[1] Tulis, A. J., and Selman, J. R., "Detonation Tube Studies of Aluminum Particles Dispersed in Air," *Proceedings of the 19th International Symposium on Combustion*, Combustion Inst., Pittsburgh, 1982, pp. 655–663.

[2] Borisov, A. A., Khasainov, B. A., Saneev, E. L., Formin, I. B., Khomik, S. V., and Veyssiere, B., "On the Detonation of Aluminum Suspensions in Air and in Oxygen," *Dynamic Structure of Detonation in Gaseous and Dispersed Media*, edited by A. A. Borisov, Kluwer Academic, Dordrecht, The Netherlands, 1991, pp. 215–253.

[3] Zhang, F., Grönig, H., and van de Ven, A., "DDT and Detonation Waves in Dust-Air Mixtures," *Shock Waves*, Vol. 11, No. 1, 2001, pp. 53–71. doi:10.1007/PL00004060

[4] Khasainov, B. A., and Veyssiere, B., "Steady, Plane, Double-Front Detonations in Gaseous Detonable Mixtures Containing a Suspension of Aluminum Particles," *Progress in Astronautics and Aeronautics*, Vol. 114, AIAA, Washington, D.C., 1988, pp. 284–299.

[5] Glassman, I., *Combustion*, Academic Press, New York, 1977, pp. 168–193.

[6] Friedman, R., and Macek, A., "Ignition and Combustion of Aluminum Particles in Hot Ambient Gases," *Combustion and Flame*, Vol. 6, 1962, pp. 9–19. doi:10.1016/0010-2180(62)90062-7

[7] Davis, A., "Solid Propellants: the Combustion of Particles of Metal Ingredients," *Combustion and Flame*, Vol. 7, 1963, pp. 227–234.

[8] Pokhil, P. F., Belyayev, A. F., Frolov, Y. V., Logachev, V. S., and Kotkov, A. I., "Combustion of Powdered Metal in Active Media," Nauka, Moscow, 1972; also U.S. Air Force Foreign Technology Div., Rept. FTD-MT-24-551-73, 1973 (English translation).

[9] Foelsche, R. O., Burton, R. I., and Krier, H., "Ignition and Combustion of Aluminum Particles in $H_2/O_2/N_2$ Combustion Products," *Journal of Propulsion and Power*, Vol. 14, No. 6, 1998, pp. 1001–1008. doi:10.2514/2.5365

[10] Melcher, J. C., Burton, R. L., and Krier, H., "Combustion of Aluminum Particles in Solid Rocket Motor Flows," *Solid Propellant Chemistry, Combustion, and Motor Interior Ballistics*, edited by V. Yang, T. B. Brill, W. Z. Ren, Progress in Astronautics and Aeronautics, Vol. 185, AIAA, Washington, D.C., 2000, pp. 723–747.

[11] Melcher, J. C., Krier, H., and Burton, R. L., "Burning Aluminum Particles Inside a Laboratory-Scale Solid Rocket Motor," *Journal of Propulsion and Power*, Vol. 18, No. 3, 2002, pp. 631–640. doi:10.2514/2.5977

[12] Fontijn, A., and Felder, W., "HTFFR Kinetic Studies of $Al + CO_2 \rightarrow AlO + CO$ from 300 to 1800 K, a Non-Arrhenius Reaction," *Journal of Chemical Physics*, Vol. 67, No. 4, 1977, p. 1561. doi:10.1063/1.434986

[13] King, M. K., "Modeling of Single Particle Aluminum Combustion in CO_2-N_2 Atmospheres," *Proceedings of the 17th International Symposium on Combustion*, Combustion Inst., Pittsburgh, 1978, pp. 1317–1328.

[14] Gurevich, M. A., Lapkina, K. I., and Ozerov, E. S., "Ignition Limit of Aluminum Particles," *Combustion, Explosion and Shock Waves*, Vol. 6, No. 2, 1970, pp. 172–175.

[15] Borisov, A. A., Gelfand, B. E., Timofeev, E. I., Tsyganov, S. A., and Khomic, S. V., "Ignition of Dust Suspensions Behind Shock Waves," *Dynamics of Shock Waves, Explosions, and Detonations*, edited by, J. R. Bowen, N. Manson, A. K. Oppenheim, R. I. Soloukhin, Progress in Astronautics and Aeronautics, Vol. 94, AIAA, Washington, D.C., 1984, pp. 332–339.

[16] Boiko, V. M., Lotov, V. V., and Papyrin, A. N., "Ignition of Gas Suspension of Metallic Powders in Reflected Shock Waves," *Combustion, Explosion and Shock Waves*, Vol. 25, No. 2, 1989, pp. 67–74.

[17] Servaites, J., Krier, H., Melcher, J. C., and Burton, R. L., "Ignition and Combustion of Aluminum Particles in Shocked $H_2O/O_2/Ar$ and $CO_2/O_2/Ar$ Mixtures," *Combustion and Flame*, Vol. 125, Nos. 1–2, 2001, pp. 1040–1054. doi:10.1016/S0010-2180(01)00225-5

[18] Tanguay, V., Goroshin, S., Higgins, A., and Zhang, F., "Aluminum Particle Combustion in High-Speed Detonation Products," *Combustion Science and Technology*, Vol. 181, No. 4, 2009, pp. 670–693. doi:10.1080/00102200802643430

[19] Lynch, P., Krier, H., and Glumac, N., "A Correlation for Burn Time of Aluminum Particles in the Transition Regime," *Proceedings of the Combustion Institute*, Vol. 32, No. 2, 2009, pp. 1887–1893. doi:10.1016/j.proci.2008.06.205

[20] Lee, J. J., and Zhang, F., "Burning Properties of Aluminum in H_2O or CO_2 Gas," *Proceedings of the 20th International Colloquium on the Dynamics of Explosions and Reactive Systems* [CD-ROM], McGill Univ., Montreal, Canada, 2005.

[21] Zhang, F., Murray, S. B., and Gerrard, K. B., "Aluminum Dust-Air Detonation at Elevated Pressures," *Shock Waves*, Vol. 15, No. 5, 2006, pp. 313–324. doi:10.1007/s00193-006-0027-0

[22] Zhang, F., "Detonation in Solid Particle-Gas Flow," *Journal of Propulsion and Power*, Vol. 22, No. 6, 2006, pp. 1289–1309. doi:10.2514/1.18210

[23] Fried, L. E., Howard, W. M., and Souers, P. C., "Cheetah 2.0 User's Manual," Rev. 5, Lawrence Livermore National Lab., Rept. UCRLMA-117541, Livermore, CA, 1998.

[24] Tulis, A. J., "On Unconfined Detonation of Aluminum Powder-Air Clouds," *Proceedings of the 1st International Colloquium on Explosibility of Industrial Dusts*, edited by P. Wolanski, Warsaw Univ., Warsaw, 1984, pp. 178–186.

[25] Ingignoli, W., Veyssiere, B., and Khasainov, B. A., "Study of Detonation Initiation in Unconfined Aluminum Dust Clouds," *Gaseous and Heterogeneous Detonations*, edited by G. Roy, S. Frolov, K. Kailasanath, N. Smirnov, ENAS Publishers, Moscow, 1999, pp. 337–350.

[26] Zhang, F., Gerrard, K., Ripley, R., and Tanguay, V., "Unconfined Aluminum Particles-Air Detonation," *Proceedings of the 26th International Symposium on Shock Waves*, Deutsches Zentrum för Luft- und Raumfahrt, Göttingen, Germany, 2007, pp. 1241.1–1241.6.

[27] Benkiewicz, K., and Hayashi, A. K., "One-Dimensional Parametric Studies of an Aluminum-Dust Combustion Model for Numerical Simulations of Detonation Waves," *AIAA Journal*, Vol. 44, No. 3, 2006, pp. 608–619. doi:10.2514/1.20412

[28] Benkiewicz, K., and Hayashi, A. K., "Two-Dimensional Numerical Simulations of Multi-Headed Detonations in Oxygen-Aluminum Mixtures Using an Adaptive Mesh Refinement," *Shock Waves*, Vol. 13, No. 5, 2003, pp. 385–402. doi:10.1007/s00193-002-0169-7

[29] Veyssiere, B., Khasainov, B. A., and Briand, A., "Investigation of Detonation Initiation in Aluminum Suspensions," *Shock Waves*, Vol. 18, No. 4, 2008, pp. 307–315. doi:10.1007/s00193-008-0136-z

[30] Fedorov, A. V., and Khmel, T. A., "Numerical Simulation of Formation of Cellular Heterogeneous Detonation of Aluminum Particles in Oxygen," *Combustion, Explosion and Shock Waves*, Vol. 41, No. 4, 2005, pp. 435–448. doi:10.1007/s10573-005-0054-7

[31] Fedorov, A. V., and Khmel, T. A., "Formation and Degeneration of

Cellular Detonation in Bidisperse Gas Suspensions of Aluminum Particles," *Combustion, Explosion and Shock Waves*, Vol. 44, No. 3, 2008, pp. 343–353.
doi:10.1007/s10573-008-0042-9

[32] Zhang, F., Frost, D. L., Thibault, P. A., and Murray, S. B., "Explosive Dispersal of Solid Particles," *Shock Waves*, Vol. 10, No. 6, 2001, pp. 431–443.
doi:10.1007/PL00004050

[33] Zhang, F., "Detonation of Gas-Particle Flow," *Heterogeneous Detonation*, edited by F. Zhang, Springer, Berlin, Apr. 2009, Chap. 2.

[34] McBride, B. J., and Gordon, S., "Computer Program for Calculating and Fitting Thermodynamic Functions," NASA Rept. RP-1271, 1992.

[35] Ripley, R. C., Lien, F., and Zhang, F., "An Approximate Riemann Solver for Multiphase Gas-Solid Flow," *Shock Waves* (submitted for publicaiton).

[36] Strauss, W. A., "Investigation of the Detonation of Aluminum Powder-Oxygen Mixtures," *AIAA Journal*, Vol. 6, No. 9, 1968, pp. 1753–1757.
doi:10.2514/3.4855

[37] Baker, E. L., Capellos, C., and Stiel, L. I., "Generalized Thermodynamic Equation of State for Reacting Aluminized Explosives," *Proceedings of the 13th International Detonation Symposium*, Office of Naval Research, Rept. ONR 351-07-01, Arlington, VA, 2006, pp. 1161–1170.

[38] Yoshinaka, A., Zhang, F., and Wilson, W. H., "Effect of Shock Compression on Aluminum Particles in Condensed Media," *Shock Compression of Condensed Matter–2007*, edited by M. Elert, M. D. Furnish, R. Chau, N. Holmes, and J. Nguryen, American Physical Society, Melville, NY, 2007, pp. 1057–1060.

J. Powers
Associate Editor